





Dynamics for the Haldane phase in the bilinear-biquadratic model

Arya Dhar ^{1,2}, Daniel Jaschke ¹ and Lincoln D. Carr ^{1,3}

¹*Department of Physics, Colorado School of Mines, Golden, Colorado 80401, USA*

²*Institut für Theoretische Physik Leibniz Universität Hannover, Appelstrasse 2, 30167 Hannover, Germany*

³*Quantum Engineering Program, Colorado School of Mines, Golden, Colorado 80401, USA*

 (Received 28 February 2021; revised 23 January 2022; accepted 16 February 2022; published 25 March 2022)

The bilinear-biquadratic model is a promising candidate to study spin-1 systems and to design quantum simulators based on its underlying Hamiltonian. The variety of different phases contains among other valuable and exotic phases the Haldane phase. We study the Kibble-Zurek physics of linear quenches into the Haldane phase. We outline ideal quench protocols to minimize defects in the final state while exploiting different linear quench protocols via the uniaxial or interaction term. Furthermore, we look at the fate of the string order when quenching from a topologically nontrivial phase to a trivial phase. Our studies show this depends significantly on the path chosen for quenching; for example, we discover quenches from Néel to Haldane phase which reach a string order greater than their ground state counterparts for the initial or final state at intermediate quench times.

DOI: [10.1103/PhysRevB.105.094309](https://doi.org/10.1103/PhysRevB.105.094309)

I. INTRODUCTION

The last three decades have witnessed an unprecedented progress [1] in fulfilling Feynman's vision of constructing a quantum simulator which would be able to solve quantum mechanical problems directly [2]. One popular approach to achieve this goal is adiabatic quantum computing, which relies on the preparation of the ground state of a Hamiltonian that is easy to attain experimentally. The system is then evolved adiabatically to the final Hamiltonian whose ground state encodes the solution to a particular computational or optimization problem [3]. Adiabatic quantum computing has been used in the D -wave architecture and is strongly related to quenches through a quantum critical point and spin-1/2 models. However, we are not constrained to spin-1/2 systems: spin-1 and beyond have even more intriguing features.

Quantum phases are usually characterized by local order parameters, and phase transitions are then described by symmetry breaking according to Landau's theory. However, there is a different class of phases called *topological phases* which are characterized by nonlocal order parameters. These phases often have a gap in the bulk energy spectrum with gapless modes residing at the edges. Furthermore, a new class of topological phase was discovered in the last decade possessing symmetry-protected topological order in which the gapless edge excitations are preserved by symmetries [4,5]. A paradigmatic example of a symmetry-protected topological (SPT) phase is the Haldane phase exhibited by the Heisenberg model with odd integer spins [6]. This phase is protected by three symmetries: time-reversal, spatial inversion, and $Z_2 \times Z_2$ symmetry. The phase possesses a nonlocal string order. These SPT phases have become potential candidates for measurement-based quantum computation for which SPT order ensures the perfect operation of the identity gate [7,8]. There have also been proposals to use SPT phases as adiabatic quantum transistors which are universal adiabatic quantum

computing devices whose operational speed depends on the minimal energy gap [9,10]. These proposed logic gates, due to their symmetry-protected feature, have been argued to be quite robust against a variety of relevant noise processes. Recently, a metrological application with the Haldane insulator was proposed in which the passive, error-preventing properties of the SPT phase can be used to measure the direction of an unknown electric field [11].

Ultracold gases loaded in optical lattices offer an exceptionally high degree of controllability over the geometry and interactions as well as time-dependent quenches. Recent years have seen a remarkable development in the variety of nonequilibrium experiments achieved by the ultracold gases such as studying their transport properties [12,13], thermalization [14], many-body localization [15,16], relaxation dynamics [17], and quench dynamics across a phase transition [18,19]. The recent realization of quantum integer-spin chains with tunable interactions using trapped ions opens up possibilities to study SPT phases in spin-1 systems [20]. Ultracold molecules represent an alternative way to achieve these effective three-level systems, also called qutrits, via the large number of hyperfine levels and the electric dipole moment [21,22]. External magnetic and laser fields can control the various interaction terms appearing in the desired Hamiltonian and perform slow to fast quenches. The development of the quantum gas microscope with single site and spin resolution will grant access to the measurement of the local and nonlocal order parameters [23–25].

The rapid development in the field of quantum computation and its relation to the SPT phases, such as the Haldane phase, and the subsequent progress in experimental endeavors have prompted us to analyze in detail quench dynamics across quantum critical points in the spin-1 bilinear-biquadratic model (BBM) associated with the Haldane phase [26–30]. Spin-1 models, i.e., qutrits, also enable more powerful applications due to more internal degrees of freedom per site [31]. In spite of many theoretical predictions, the Haldane

phase has remained elusive in experiments. Through careful analysis, we propose in this article the parameters for linear quench protocols which minimize defect generation and thus will provide experimentalists a route to observe the Haldane phase with a finite string order. The fate of string order when quenching is examined through different pathways to a topologically nontrivial phase; up till now, the dynamics of the Haldane phase has still not been studied in much detail. Apart from the experimental stimulus, there is also the motivation of relating defect generation to the quench speed. For quenches across second-order phase transitions, the Kibble-Zurek hypothesis proposes a universal nature of the density of defects, relating them to the critical exponents of the underlying quantum phase transition. We analyze the statics and dynamics of the BBM with the matrix product state (MPS) method [32] which is well-suited for 1-dimensional entangled many-body systems and gives us access to a variety of relevant measures that can be pivotal in the analysis.

The paper is arranged as follows: We begin with the definition of the BBM in Sec. II, also containing a general discussion of the Kibble-Zurek mechanism. The results of the different quench protocols to the Haldane phase are presented in Sec. III. We elaborate the methods, a detailed error analysis, and the static results for finite-size systems in Sec. IV. Finally, Sec. V concludes our work with discussion.

II. MODEL

Although our results are general to many quantum simulator architectures, we contextualize our study with the specific architecture of an ultracold spin-1 bosonic gas trapped in a 1-dimensional optical lattice with repulsive interactions between them. Because of the identity of bosons undergoing an s -wave interaction, the total spin of the two interacting bosons, S_{tot} , can be 0,2. If the tunneling amplitude t between neighboring lattice sites is small and finite, one can apply a second-order perturbation theory in t to get the low-energy physics which is given by the superexchange processes. The corresponding spin Hamiltonian for two neighboring sites at unit filling can be expanded in powers of the nearest-neighbor Heisenberg interactions, $H_{i,i+1} = \sum_k a_k (\mathbf{S}_i \cdot \mathbf{S}_{i+1})^k$. Terminating the series at $k = 2$, i.e., second-order perturbation theory, gives the BBM, up to the external field which is often also included in the BBM. The presence of a symmetry-breaking field can have important consequences. The linear Zeeman effect does not play a role since it can be gauged out due to the fact that the total magnetization is a constant of motion. It should be noted that this symmetry is used as well for the numerical simulations. On the other hand, the quadratic Zeeman effect leads to effects in spinor gases which cannot be gauged away. Combining the two effects leads us to the BBM with quadratic Zeeman field:

$$\mathcal{H} = J \sum_{i=1}^{L-1} \left[\cos(\theta) \mathbf{S}_i \cdot \mathbf{S}_{i+1} + \sin(\theta) (\mathbf{S}_i \cdot \mathbf{S}_{i+1})^2 \right] + D \sum_{i=1}^L \hat{S}_i^z{}^2, \quad (1)$$

where $\mathbf{S}_i = (\hat{S}_i^x, \hat{S}_i^y, \hat{S}_i^z)$ are the angular momentum operators located at the i th site of a 1D L -site qutrit, or spin-1 lattice. The first sum in Eq. (1) is the bilinear-biquadratic part tuned by the parameter θ , whereas the second term is the uniaxial field D taking into account the quadratic Zeeman field. Some of the phases exhibited by Eq. (1) have degenerate ground states. Hence, for the purposes of numerical calculations, a very small symmetry-breaking field is applied to the L th site.

The Hamiltonian in Eq. (1) obeys a $\mathcal{U}(1)$ symmetry similar to the number conservation in the Bose-Hubbard model, where here the total spin in the z direction is conserved. The generator of the symmetry is $\oplus_{i=1}^L \hat{S}_i^z$. Thus, the possible symmetry sectors reach from a total z spin of $-L$ to $+L$. We use a total spin of zero throughout our simulations with open boundary conditions. We follow the convention that the time is in units of the interaction J .

The BBM has been extensively studied revealing a plethora of phases such as the dimer phase, the Néel phase, and the Haldane phase, to name a few [30]. Due to the high relevance in recent experiments with ultracold gases in optical lattices [25,33], we study the effects of quenches across the following phase boundaries shared by the Haldane phase:

- (A) Néel and Haldane phase.
- (B) Large- D (non-Haldane) and Haldane phase.

The critical points for the respective quantum phase transitions for the specific lengths of the systems are first determined using the respective order parameters. The linear quenches start and finish almost equidistant from the corresponding critical points on either side. We ensure that the initial and final points are deep inside the respective phases, so that the effects of the critical region are properly considered.

The effects of the linear quench, crossing the quantum critical point in the process, are examined via the following six observables:

- (1) The *instantaneous energy gap* is a static measure characterizing the difference between the ground state energy E_0 of the system and the energy E_k of the k th relevant excited state compatible with the integrals of motion

$$\Delta_{0k} = E_k - E_0. \quad (2)$$

The choices of the ground and relevant excited state considered for this measure always belong to the same symmetry sector, i.e., have the same spin projection in the z direction.

- (2) The *staggered magnetization* is defined as

$$M_z^{\text{st}} = \frac{1}{L} \sum_{i=1}^L (-1)^i \hat{S}_i^z. \quad (3)$$

The Néel phase is characterized by a finite value of the staggered magnetization.

- (3) The *entanglement entropy*, also called *block entropy*, is a measure defined based on the reduced density matrix or Schmidt decomposition, i.e.,

$$S = -\text{Tr}_B \rho_{AB} \ln \rho_{AB} = -\text{Tr}_A \rho_A \ln \rho_A, \quad (4)$$

where ρ_A is the reduced density matrix of the subsystem A by tracing over the degrees of freedom of the rest of the system, i.e., subsystem B . Throughout our work, we choose subsystem A as the sites $1, \dots, L/2$ with L being even; the

sites $L/2 + 1, \dots, L$ represent the subsystem B with the degrees of freedom being traced out. Typically, the entanglement entropy scales with the size of the subsystem, $n_A \equiv L/2$ [34]. However, in one-dimensional systems with only short-ranged terms in the Hamiltonian, the entanglement entropy saturates to a constant value independent of the size of the block. This property, known as the ‘‘area law’’ [35], is the cause behind the remarkable success of tensor-network-based methods in describing 1-dimensional systems. In the vicinity of a quantum critical point, the entanglement entropy starts to diverge logarithmically with the block size n_A for large system sizes, as

$$S \sim c \ln(n_A), \tag{5}$$

where c is the central charge of the conformal field theory describing the critical point [36–39]. For systems slightly away from the critical point, when the correlation length ξ in the ground state is large but finite, the entanglement entropy behaves as

$$S \sim \mathcal{A} \frac{c}{6} \ln \xi, \tag{6}$$

where \mathcal{A} is the number of boundary points of the system.

(4) We consider the reduced density matrix of a subsystem, or alternatively, the eigenvalues of the bipartitions, via the singular values of the Schmidt decomposition, where the *Schmidt gap* is defined as

$$\Delta\lambda = \lambda_1 - \lambda_2, \tag{7}$$

with λ_1, λ_2 the highest two eigenvalues of the reduced density matrix. Using finite-size scaling, the Schmidt gap can signal a quantum phase transition. $\Delta\lambda$ scales with the critical exponents related to the conformal field theory describing the transition point [40]. References [40,41] have recently shown that the Schmidt gap is related to the correlation length of the system, ξ , through a power law, where the exponent is called the dynamical critical exponent of the transition. Studying the complete entanglement spectrum in a dynamical problem can be complicated. Since both entanglement entropy and the Schmidt gap are related to the entanglement spectrum and give equivalent insights, we concentrated on these two established quantities.

(5) The *string order parameter* is a nonlocal measurement acting on multiple sites defined as

$$O^S = \lim_{L \rightarrow \infty} O_i(r = L - 2i) \\ \equiv \lim_{r \rightarrow \infty} \left\langle \hat{S}_i^z \exp \left[i\pi \sum_{j=i+1}^{i+r-1} \hat{S}_j^z \right] \hat{S}_{i+r}^z \right\rangle, \tag{8}$$

where the imaginary unit is i and the site index is i . The string order parameter is an effective nonlocal operator to characterize hidden orders present in quantum phases of matter that cannot be described by the typical local operators [6,42–44]. The string order has shown signatures of thermalization for scales related to the Lieb-Robinson bound [45]. The remnant string order at finite times after a sudden quench out of the Haldane phase was credited to the preservation of symmetries of the Hamiltonian [45]. However, if the symmetry is broken in the new phase after the sudden quench, then the string order is

lost even at infinitesimal times in the thermodynamic limit. Such behavior makes the string order qualitatively different from the standard local order parameters [46]. In the case of finite systems, we measure $O_i(r = L - 2i)$, where $i = 10$; this approach avoids boundary effects.

(6) The *excess energy* measures the degree of excitation in the time-evolved states as

$$\Delta E(\tau) = E_f - E_f^g, \tag{9}$$

where $E_f = \langle \psi(\tau) | \mathcal{H}(\tau) | \psi(\tau) \rangle$ is the energy of the system described by $|\psi(\tau)\rangle$ after evolving through the quench time τ , and E_f^g is the ground state energy of the final Hamiltonian, $\mathcal{H}(\tau)$. The excess energy is equal to the weighted sum of all the excitation energies. As a result, this quantity will serve as the analog of the defect density originally considered by Kibble and Zurek [47–50].

Some of the above quantities can be related to the speed of the quench in a universal manner through the well-known Kibble-Zurek mechanism.

This mechanism was originally proposed by Kibble in the context of defects generated in the early universe [51], which was later extended by Zurek to condensed matter systems [52,53]. This mechanism describes the formation of topological defects when the system is ramped slowly across a second-order critical point, where the defect density depends on the ramp rate exponentially. The exponents in such a dependence were shown to be related to the universal equilibrium exponents of the underlying quantum phase transition. Because of the divergence of the correlation length in the vicinity of the critical point, it is impossible to ramp the system across the critical point adiabatically without the formation of defects, thus signaling the breakdown of the adiabatic theorem.

Without loss of generality, we can consider a linear quench, such as

$$\epsilon(t) = \epsilon_0 + \frac{(\epsilon_f - \epsilon_0) \cdot t}{\tau}, \quad 0 \leq t \leq \tau, \tag{10}$$

where ϵ is the quench parameter as a function of time t , ϵ_0 and ϵ_f are the initial and final values of the parameter before and after the quench, and τ is the time for quench. The parameter $\epsilon(t)$ can be D, θ , or a linear combination of both. Scaling analysis of the divergence of the correlation length ξ shows that any quantity which is related to the correlation length or the defect density, i.e., the excess energy, will depend on the quench rate polynomially, with the exponent being a combination of the critical exponents of the transition. While tuning the critical exponents to be evaluated with the aim of making the rescaled curves for different system sizes fall together is well established in the statics, the time evolution relies on fitting the defect density or excess energy [53]. The defect density n_{ex} follows the relation

$$n_{ex} \sim \tau^{d\nu/(1+z\nu)}, \tag{11}$$

where d is the dimension of the system considered, and z and ν are the critical exponents of the transition. The scaling in Eq. (11) has been observed in many quench protocols, but it should also be noted that there are systems where such a scaling analysis fails [54,55]. For example, there are some

bosonic systems which remain nonadiabatic in the thermodynamic limit.

The scaling analysis of Eq. (11) presumes the thermodynamic limit when the correlation length diverges to infinity at the critical point. However, in finite-sized systems, the maximum value of the correlation length can be the system size. Following a similar argument proposed by the Kibble-Zurek mechanism, the minimum quench time needed for the system to attain adiabaticity is given by

$$\tau_{\min} = L^{z\nu/(1+z\nu)}. \quad (12)$$

It is thus important to check for the validity of the Kibble-Zurek mechanism in the BBM. We do so by performing a linear quench across the phase transition and checking for estimates of the τ_{\min} such that the final time-evolved state is close to the ground state in the Haldane phase. Since the excess energy, ΔE , is a measure for the density of defects formed in the system, we can use Eq. (11) by replacing n_{ex} with ΔE when checking for the validity of the Kibble-Zurek mechanism.

Quantities such as the Schmidt gap and entanglement entropy are related to the correlation length, and hence will scale with the quench time following the Kibble-Zurek mechanism as

$$\Delta\lambda \sim \tau^{-z\nu/(1+z\nu)}, \quad (13)$$

$$S = \frac{\mathcal{A}c\nu}{6(1+z\nu)} \ln \tau + \text{const.} \quad (14)$$

For finite-size systems, a subsystem has two boundaries, and hence $\mathcal{A} = 2$ [38,56,57].

III. QUENCHING TO THE HALDANE PHASE

In this work, we concentrate on reaching the Haldane phase from the Néel phase and the large- D phase since these phases can be easily prepared in experiments with high fidelity. We choose representative quantum critical points and perform a linear quench across the respective quantum critical points as shown schematically in Fig. 1.

We begin the quench sufficiently far away from the quantum critical point and terminate the quench process approximately equidistant from the critical point on the other side. The quench time is then varied to study its effects on the quench processes. In addition, the system-size dependence is studied by scaling up to systems as large as 200 sites. We categorize the results according to the selected quantum phase transitions: Secs. III A and III B for linear quenches from Néel and large- D to Haldane phase, respectively.

A. Néel to Haldane phase

The Néel phase is characterized by a finite nonzero spontaneous staggered magnetization M_z^{st} . On the other hand, the Haldane phase represents a topological phase in a 1-dimensional system signaled by a finite string order defined in Eq. (8). The Haldane phase also displays a degeneracy in the entanglement spectrum, given by the Schmidt gap as defined in Eq. (7). Using a finite-size scaling of the staggered magnetization acting as the order parameter, the phase boundary

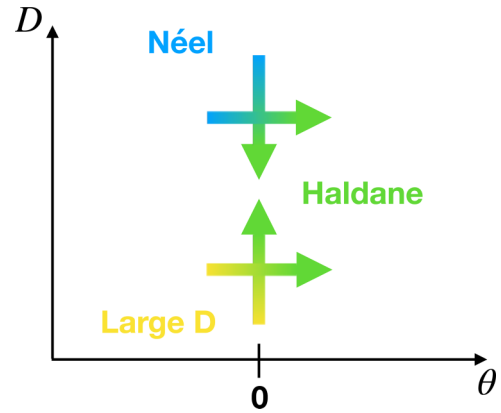


FIG. 1. Schematic phase diagram: Our studies encompass quenches of either the external field D or the interaction θ . The phase diagram contains the Néel to Haldane phase transition, and the large- D phase to Haldane transition. The exact values of the phase boundaries depend on finite-size effects and differ for the range of system sizes that we consider in our simulations; a thorough study may be found in [30].

separating these two quantum phases has been identified in an earlier work [30]. Therein, finite-size scaling analysis of the staggered magnetization and Schmidt gap yields the critical exponent $\nu = 1.01$, consistent with the Ising universality class, $\nu_{\text{Ising}} = 1$ [30,58,59]. For an Ising transition, the critical exponent, $z = z_{\text{Ising}} = 1$ is known. However, for the present transition from Néel to Haldane phase, the value of z has not been calculated explicitly and numerically.

We perform a linear quench on the uniaxial field D and keep the interaction θ fixed to 0 during the time evolution. We ensure that the initial and final values of D are such that they correspond to Néel and Haldane phase, respectively, and are far away from the quantum critical region.

We first look at the excess energy ΔE the system acquires when quenched across the quantum critical point, as defined in Eq. (9). ΔE is proportional to the number of defects formed in the system after the quench, and hence is expected to display Kibble-Zurek-like scaling [60]. The behavior of ΔE as a function of the quench time τ is plotted in Fig. 2 for two different system sizes. Three distinct regimes can be seen from the plots. ΔE saturates to its maximum value for very fast quenches, i.e., low values of τ . This observation is consistent with the fact that there can be a maximum number of excitations in the system after the quench due to its finite size. The final state after the time evolution is thus a superposition of several excited states. The value of ΔE for the same value of τ increases with the system size indicating a larger number of defects in the system is formed after the quench for bigger systems. This expected trend is due to the inverse dependence of the energy gap on the system size at the critical point. For larger system sizes, the gap is smaller; a smaller energy gap enhances the probability of exciting the system to higher excited states, which leads to a larger number of defects.

For very large values of τ , applying the effective Landau-Zener model would have resulted in a scaling of $\Delta E \sim \tau^{-2}$, e.g., see [53,60]. However, as shown in Fig. 2, we do not quite

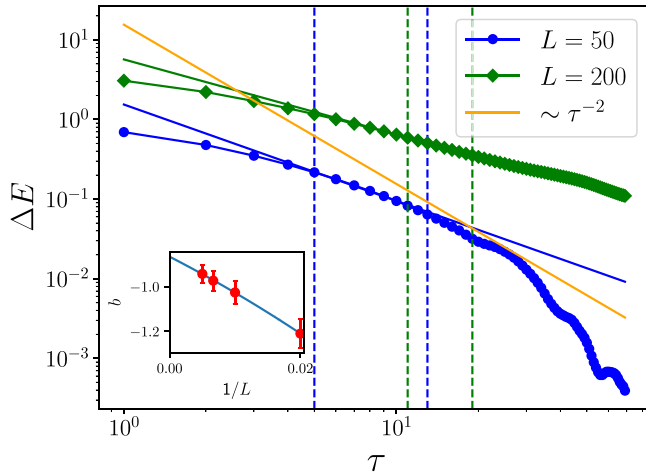


FIG. 2. Excess energy ΔE as a function of quench times τ for two different lengths $L = 50, 200$. We quench the uniaxial field from $D_i = -0.5$ to $D_f = -0.15$; the interaction terms are constant at $\theta = 0$. The dashed lines denote the region where the excess energy, ΔE , is fitted by a power-law for the respective system sizes. The orange line denotes an inverse quadratic function, $\Delta E \sim \tau^{-2}$. Inset: The values of Kibble-Zurek exponent $b(L)$, extracted by fitting a power-law to the excess energy in the intermediate τ values for different system sizes, L , plotted as a function of the inverse system size $1/L$. A quadratic fit was employed to extrapolate an estimate for the thermodynamic limit, b_∞ .

observe such a behavior. We would explore the presence of the Landau-Zener effect for higher values of τ for the system sizes considered, but such simulations are beyond the scope of the current numerical techniques because of the large error involved. In contrast, we observe the decay at large τ superimposed by oscillations for $L = 50$. These oscillations naturally arise when effects of finite duration time are considered [60–62]. The frequency of the oscillations decreases with increasing system size, along with a shift to higher quench times where the oscillations are dominant. The oscillatory behavior can be suppressed by increasing the distance of the initial value D_i from the critical D_c compared to the width of the critical regime [60]. The intriguing quasiadiabatic region lies between these two regimes where the residual energy follows a power-law behavior. We attempt to verify the Kibble-Zurek mechanism for this quench protocol. For different lengths, we fit a power law in the intermediate power-law regime,

$$\Delta E = a\tau^{b(L)}. \quad (15)$$

The value of the exponent $b(L)$ calculated through the exponential fitting procedure for different system sizes L is then fitted using a quadratic scaling resulting in an asymptotic value of $b_\infty \sim -0.866 \pm 0.008$ (see Fig. 2) for $L \rightarrow \infty$. The error bars include the errors arising from the fitting procedure due to the range of τ values used to fit and the fit itself.

The phase transition from Néel to Haldane phase along the D axis belongs to the Ising universality class concluded from previous finite-size-scaling studies with the staggered magnetization and Schmidt gap [30,41]. We insert the corresponding critical exponents $\nu_{\text{Ising}}, z_{\text{Ising}}$ in Eq. (11) and obtain a value of $b_{\text{theoretical}} = 0.5$. This number is quite different from

the estimate extracted from our present numerical calculations using excess energy b_∞ . The discrepancy can arise for two different reasons: either the Kibble-Zurek mechanism is not valid for this transition or the critical exponents are incorrect. Before coming to the conclusion that the Kibble-Zurek mechanism fails to describe the transition, let us try to verify all the critical exponents appearing in Eq. (11). Since ν has been rigorously calculated using the density matrix renormalization group (DMRG) method and quantum Monte Carlo simulations, the only quantity that remains unknown is the critical exponent z since $d = 1$. Assuming the Kibble-Zurek scaling to be valid, and inserting the value of b_∞ , we can estimate $z = 0.159$. Using this value of z , we can see if other quantities such as the Schmidt gap and the entanglement entropy behave consistently according to the Kibble-Zurek mechanism with the obtained value of z . It should be noted that the possibility of anomalous Kibble-Zurek scaling exists as reported earlier for quenches across topological phases with edge states [63] which is robust to defect formation. However, that is unlikely the case here since we are quenching from a nontopological phase to a topological phase.

We point out that the reverse quench protocol, i.e., from the Haldane to the Néel phase, finds a similar power-law behavior of the excess energy in the intermediate regime of quench times. We performed additional simulations to verify this observation, not shown here for brevity.

The Schmidt gap and the block entropy, as defined in Eqs. (7) and (4), are analyzed for the same quench protocol from Néel to Haldane phase by changing D ; see Fig. 3. Due to the dependency of both quantities on the correlation length, they should also follow a Kibble-Zurek scaling. Assuming the Kibble-Zurek scaling is valid for this transition, inserting the values obtained from the scaling of excess energy into Eq. (13) leads to the following scaling of the Schmidt gap:

$$\Delta\lambda \sim \tau^{-0.138}. \quad (16)$$

Periodic oscillations are observed for a given system size in the Schmidt gap related to crossings of the first two eigenvalues in the entanglement spectrum, with an overall decay. This decay is power law in nature with an exponent agreeing with Eq. (16). The cusps in the Schmidt gap are related to the periodic nonanalyticities of the free-energy density in the thermodynamic limit [64]. The cusps are not an artifact of finite-size effects since the positions of the cusps converge to one value for system sizes larger than 100. A similar behavior of the Schmidt gap has been reported earlier [57,64] indicating the signature of a dynamical phase transition.

The block entropy for small quench times, i.e., $\tau \leq 10$, coincides for all the lengths considered in our simulations. This observation implies that the entanglement spread has occurred on a length scale much smaller than any of the system sizes considered in this work. Thus, we can set a lower limit on the ramp velocities, i.e., the inverse of τ , for which the size of the system does not play an important role in the formation of entanglement. For $\tau > 10$, the data for $L = 50$ deviates from the larger lengths: the entropy abruptly jumps to a higher value. We note as expected that such a separation for larger lengths is also observed in the Schmidt gap behavior. The block entropies for the large lengths continue to show a remarkable coincidence for significantly higher values of τ .

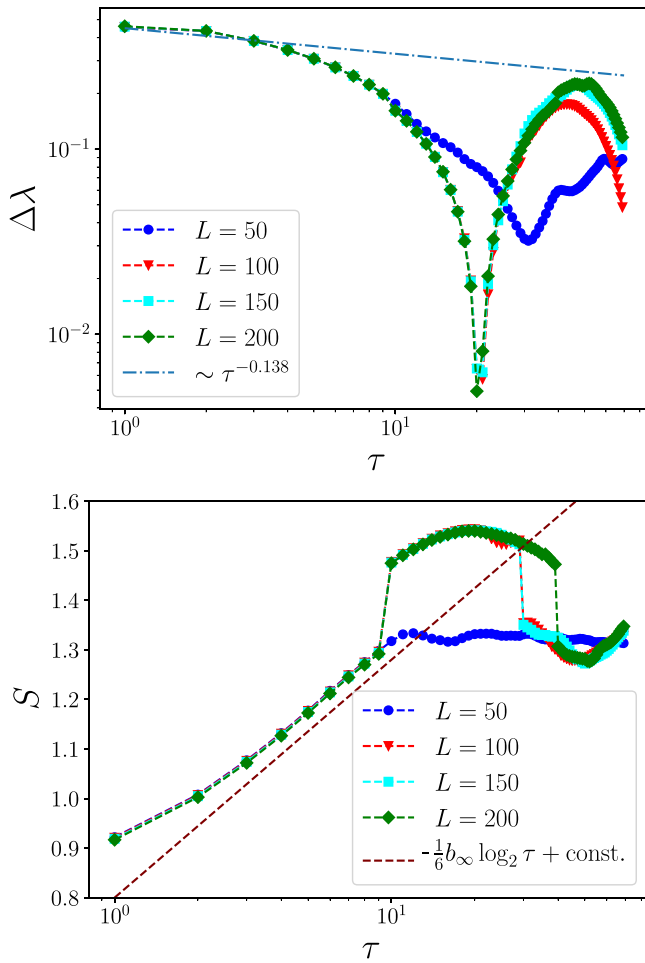


FIG. 3. Schmidt gap $\Delta\lambda$ (top) as a function of the quench time τ for different lengths L displays cusps related to the nonanalytic behavior of the free-energy density. Bottom: Block entropy S as a function of τ for the same quench parameters as above. The maroon dashed curve in the plot of the block entropy corresponds to the Kibble-Zurek scaling from Eq. (14). The quench protocol is similar to that shown in Fig. 2.

The peak value at $\tau \approx 50$ in this regime occurs at the τ value for which we observed the cusps in the Schmidt gap in Fig. 3.

To check the validity of the Kibble-Zurek mechanism, we insert $\nu = 1.01$ and $z = 0.159$ in Eq. (14) with $c = 1/2$ [40,57]. The logarithmic behavior is clearly seen for all system sizes for $\tau < 10$ in Fig. 3; thus, we confirm the Kibble-Zurek behavior of the entanglement entropy. As expected, the Kibble-Zurek prediction breaks down for smaller system sizes, i.e., $L = 50$, and larger τ values. There is an oscillatory behavior superimposed on the logarithmic behavior which arises from the oscillatory nature of the entanglement entropy. But to see the oscillations clearly, quenches with larger τ values need to be simulated; these simulations are beyond the scope of this work. Both the Schmidt gap and block entropy verify our initial assumption of the Kibble-Zurek mechanism to be valid, and hence the value of z deduced from our calculations for this particular phase transition from Néel to Haldane phase is proved to be correct.

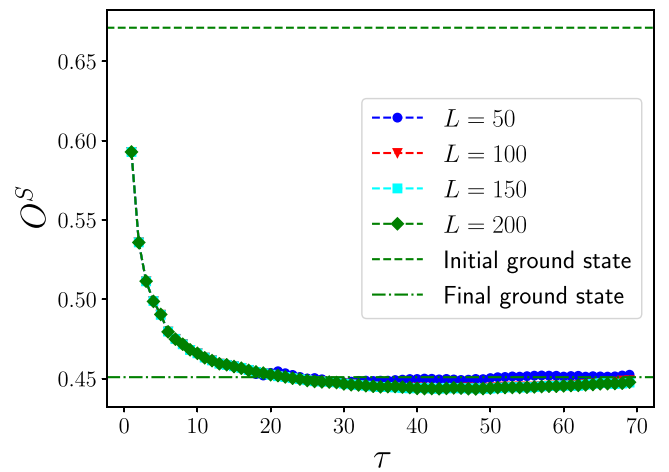


FIG. 4. String order O^S after a time evolution τ for different lengths L decreases for slower quenches and becomes equal to the ground state value of the final Hamiltonian. The quench protocol is similar to that shown in Fig. 2. The initial (green dashed) and final (green dot-dashed) ground state values for the largest system size are shown for comparison.

Both the initial and final phases display a finite string order, although deep in the Néel phase the string order is higher than in the Haldane phase. Quenching from the Néel to the Haldane phase, the time-evolved state is expected to generate defects since it crosses the quantum critical point. We consider it worthwhile to study the fate of the string order after the quench in D as shown in Fig. 4. We observe that for approximately $\tau > 20$, the string order attains a value very close to that of the ground state of the final Hamiltonian for all the system sizes. We can thus conclude that the string order converges to the final ground state value very quickly compared to the other observables shown before. This result indicates the possibility of creating the Haldane insulator phase experimentally. One needs to first prepare the Néel phase, which has already been achieved in experiments [65], and then quench D with $\tau > 20$ to reach the Haldane insulator phase for system sizes considered here. The quench process will not excite the system enough to kill the string order, as reported in earlier theoretical works with sudden quenches [45,46].

The quench from the Néel to the Haldane phase can also be achieved along the θ direction. Figure 5 shows the behavior of the excess energy as a function of the quench time after a quench by changing θ , holding D constant at -0.310 . We find a power-law region for intermediate τ values. Extrapolating the power-law exponents for different system sizes gives a value of $b_\infty = -0.873 \pm 0.011$, which is consistent with the extrapolated value obtained in the previous protocol of quenching the external field from Néel to Haldane phase, where we found $b_\infty = -0.866 \pm 0.008$.

We now look at the evolution of the string order parameter, O^S , after the quench in the θ direction in Fig. 5. Before proceeding to study the effect of the quench, it is informative to notice the ground state values. Typically the Néel phase has a larger string order compared to the Haldane phase. This observation is always true when the interaction θ is fixed and

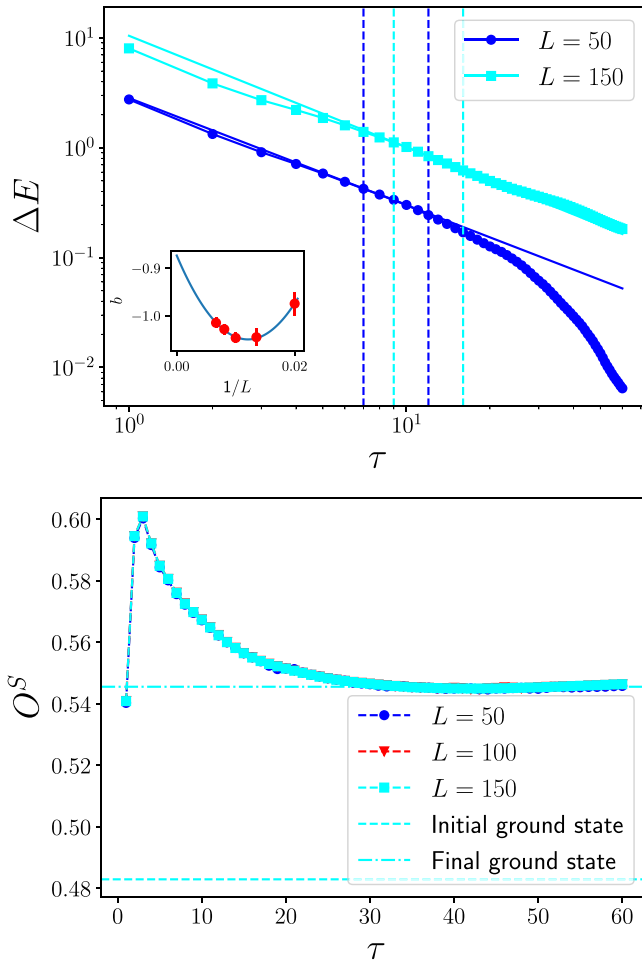


FIG. 5. Top: Quenching from Haldane to Néel phase by changing the tuning of the interaction θ from -0.1π to 0.1π at a constant uniaxial field of $D = -0.310$ exhibits a different behavior for excess energy ΔE with a power-law behavior denoted by the red line with the power-law exponent, $b = 0.873 \pm 0.011$ for a system size of $L = 150$. Bottom: String order O^S after the linear quench for intermediate quench times becomes higher than the final ground state value. The initial (dashed cyan line) and final (dot-dashed cyan line) ground state values of the string order are shown for comparison.

the external field D is varied. However, this statement may not be true when going from Néel to Haldane phase through other trajectories in the phase diagram. For the protocol where D is kept fixed and θ changed, we clearly see that the ground state string order in the Néel phase is smaller than in the Haldane phase. Following the linear quench, the string order converges to the ground state value of the final Hamiltonian for longer quench times; see $\tau > 30$. In contrast, we observe that for very short quench times the string order increase monotonically, till it reaches a maximum at $\tau \sim 3$. Surprisingly, for intermediate quench times ($2 < \tau < 30$), the string order after the time evolution is larger than the final ground state value. This behavior is indeed not expected, and it implies that for a certain range of quench times, the excitations are produced in such a way that enhances the final string order. This observation implies clearly that using this quench protocol the ground state of the Haldane phase may not be reached for intermediate times,

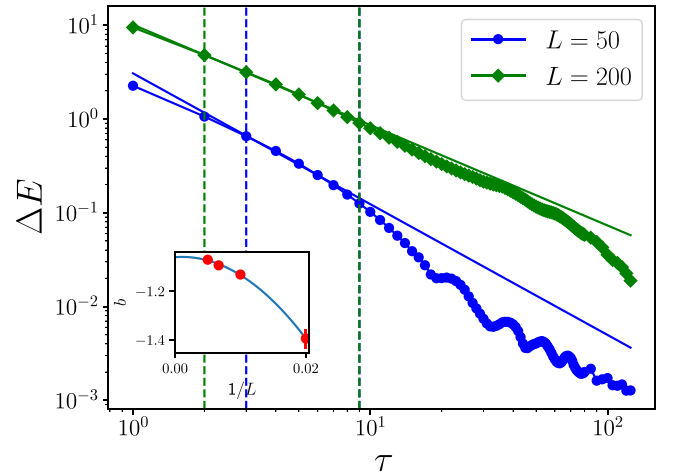


FIG. 6. Excess energy ΔE displays a power-law behavior as a function of quench time τ , shown here for two different lengths L after quenching from a uniaxial field $D_i = 1.6$ to $D_f = 0.6$; the interaction is held constant, $\theta = 0$. The vertical dashed lines denote the region which is fitted by the power law, $\Delta E = a\tau^b(L)$, for the corresponding system size, L . Inset: Quadratic extrapolation of b values for different system sizes, L , yields $b_\infty = -1.06 \pm 0.021$.

but the final state will have larger string order, offering a surprising and useful experimental prescription to maximize string order.

B. Non-Haldane (large- D) to Haldane phase

We now investigate the effects of quenching from the large- D phase to the Haldane phase as shown in the schematic Fig. 1. We follow a similar approach as before, quenching by changing D and θ . Previous studies [40] have shown that this transition has a critical exponent $\nu = 1.56$ and a central charge $c = 1$, both distinct from the values of ν and c corresponding to the transition from Néel to Haldane phase.

Figure 6 clearly shows a power-law region as expected from the Kibble-Zurek mechanism. Characteristic oscillations in the residual energy are observed for very slow quenches. Due to computational complexity, this feature is visible only for smaller lengths. Fitting the extracted value of the power-law exponent $b(L)$ in the quasiadiabatic regime with a quadratic function of the system size, we obtain $b_\infty = -1.06 \pm 0.02$. This value is certainly different than what was obtained in the previous quench protocol of Néel to Haldane phase. Since the Kibble-Zurek mechanism is valid, we can extract the critical exponent z as before. This analysis yields $z = 0.229 \pm 0.004$.

The final Schmidt gap displays cusplike behaviors arising from the nonanalyticity, but only for larger lengths, i.e., $L = 150, 200$, which can be early-time indications of dynamical phase transitions as shown in Fig. 7. If the quench is done rapidly ($\tau < 8$), the largest two eigenvalues of the reduced density matrix remain almost degenerate. However, for $L > 150$, the Schmidt gap is two orders of magnitude lower than that in the adiabatic limit ($\tau > 20$) when compared to smaller systems of $L < 100$. Due to the fact that the Schmidt gap in the final ground state is smaller than its initial ground state value, the oscillations exhibit a power-law decay envelope.

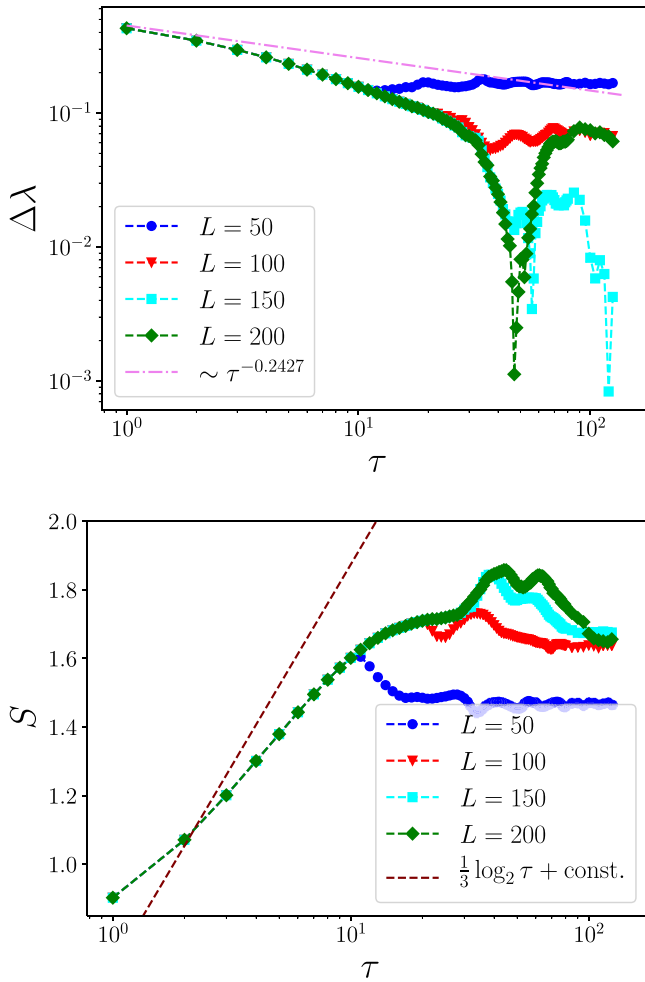


FIG. 7. Top: Schmidt gap after the quench has cusps at different quench times for larger system sizes. The pink dot-dashed line is the expected power-law envelope from Eq. (13). Bottom: The block entropy shows a marked deviation from the expected Kibble-Zurek scaling, shown by the maroon dashed line. The quench protocol is similar to that mentioned in Fig. 6.

The entanglement entropy after the time evolution shows a characteristic power-law behavior for smaller quench times, followed by oscillations. Fitting this power-law region with Eq. (14), the corresponding values for this transition do not show a good agreement. This behavior can imply either the Kibble-Zurek mechanism is not valid in this transition, and hence the z value derived is incorrect, or the entanglement entropy does not comply with the Kibble-Zurek mechanism. Deviations from the power-law behavior occur progressively at larger quench times with increasing system size. The oscillations typically occur when the power-law region ends, and can be attributed to the presence of excited components in the wave function after crossing the critical point [57].

The Haldane phase has a finite string order unlike the large- D phase. Following a quench from the large- D to Haldane phase, the string order is found to approach the final ground state value in the Haldane phase for all system sizes as shown in Fig. 8. Oscillations in the time-evolved string order as a function of the quench time in the adiabatic limit

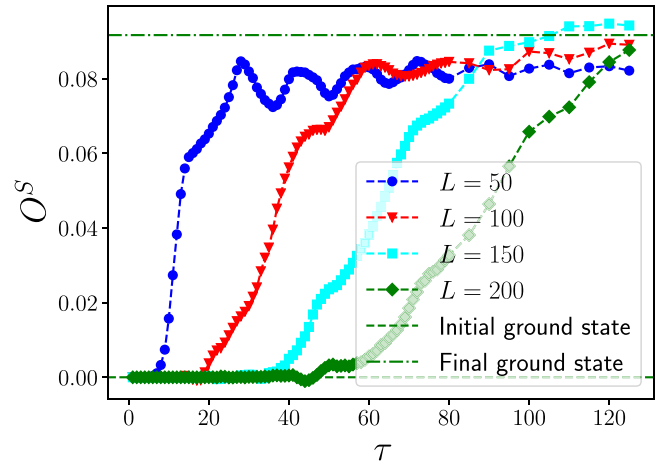


FIG. 8. Following a quench as mentioned in Fig. 6, the string order increases toward the final ground state value for slower quenches. However, larger systems require longer quench times to reach the final ground state value, shown by the green dot-dashed line.

are noticeable for smaller system sizes whereas the proximity of the converged time-evolved string order to the final ground state value increases as the system size increases. Both these effects can be attributed to finite-size effects. The quench time at which the evolved string order converges close to the final ground state value depends explicitly on the system size.

The quench from large- D to Haldane phase can also be attained by changing θ and keeping D fixed. Figure 9 shows the behavior of the excess energy as a function of quench times. Extracting the power-law exponent from the quasiadiabatic regime and extrapolating to the thermodynamic limit suggests a value of $b_\infty = -0.701 \pm 0.001$. This value is markedly different from that obtained when quenching along the external field, D , from the large- D phase to Haldane phase, suggesting

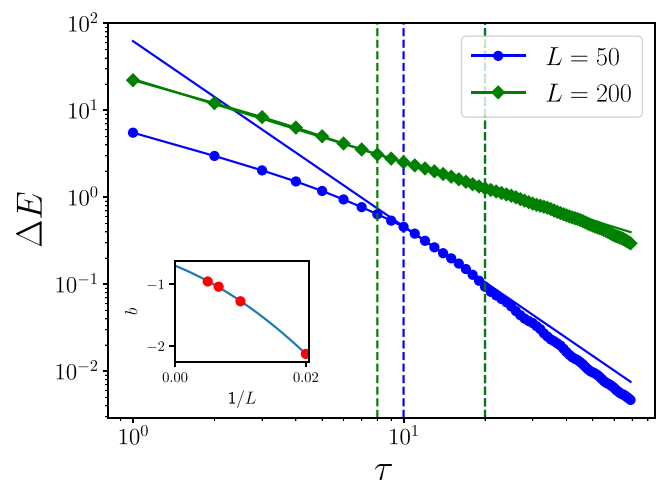


FIG. 9. Excess energy ΔE as a function of quench times τ for two different lengths L after quenching the interacting parameter from $\theta_i = -0.25\pi$ (large- D phase) to $\theta_f = 0.15\pi$ (Haldane phase); the uniaxial field is held constant at $D = 0.5$. The dashed line denotes the region which is fitted by the power law, $\Delta E = a\tau^b$. Inset: The thermodynamic value of $b_\infty = -0.701 \pm 0.001$ is obtained when $b(L)$ is fitted with a quadratic function of $1/L$.

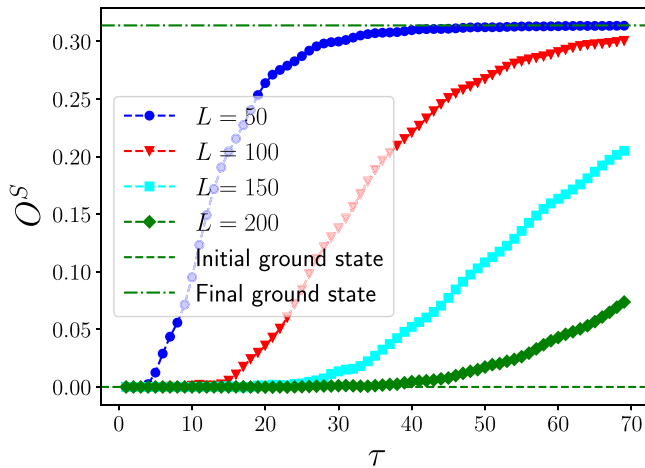


FIG. 10. String order O^S after the time evolution for different lengths L corresponding to the quench from $\theta_i = -0.25\pi$ to $\theta_f = 0.15\pi$ while holding $D = 0.5$.

a different universality class of the transition depending on the path taken from one phase to the other. Examining the string order after the quench in Fig. 10, we recognize a system-size-dependent behavior. The evolved string order reaches the final ground state value at quench times which increases with system size. Unlike the previous quench protocol, we observe neither any oscillations in the time-evolved string order nor a size-dependent difference between the ground state and the evolved string order. However, it should be noted that both the quench protocols show a system-size-dependent behavior of the string order when evolving from large- D to Haldane phase. This observation is in stark contrast to the scenario when evolving from the Néel to the Haldane phase, where the string order has no dependence on the system size. Such a behavior will be very useful for experimental groups where observations are likely to show finite-size effects.

IV. METHODS AND ERROR ANALYSIS

We used two different MPS packages to simulate the statics and dynamics of the Hamiltonian described in Eq. (1), i.e., openTEBD [66] and openMPS [67,68]. The ground state simulations were carried out with bond dimension 1000, and a maximum system size of 200 lattice sites. For the time-dependent simulations, fourth-order Suzuki-Trotter decomposition was used with typical time steps of 0.01, truncation error limit of 10^{-10} , and bond dimensions between 500 to 800 depending on the quench protocol and system size.

We support our results from the previous section with the following error analysis. Numerical simulations with tensor network methods have two main sources of error. On the one hand, we have the Trotter approximation scaling as a power of the time step dt [32]. On the other hand, we have the truncation of the Hilbert space in terms of the bond dimension. Both errors are applicable to the statics and dynamics as we use imaginary time evolution for the statics; a variational ground state does not have a Trotter error [21]. Error bounds can be calculated for observables based on the variance of the energy and the energy gap to the first excited state for

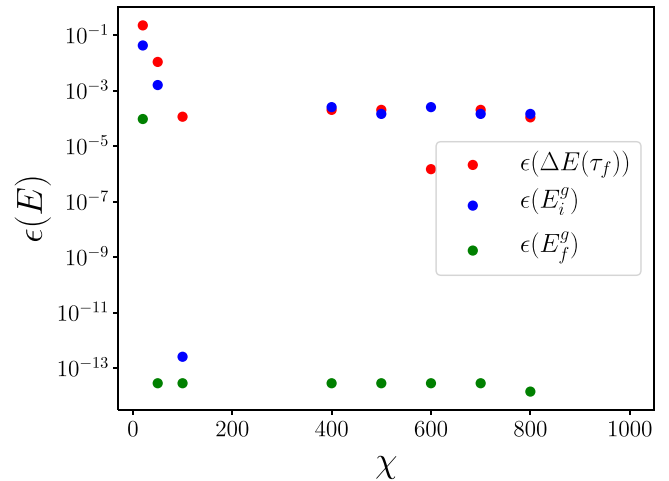


FIG. 11. Error analysis: The difference in the final energy after time evolution, the initial ground state energies, and the final ground state energies for different bond dimensions, χ , with the corresponding value obtained using the largest bond dimension, as a function of bond dimensions for Haldane phase to large- D phase quenches and a system size of 200 sites.

the ground state [67]. The n th-order Trotter decomposition has a well-controlled error proportional to $\mathcal{O}(dt^n)$. Thus, we concentrate in the following on the bond dimension, where the maximum grows exponentially with the system size. The validity of a truncation to a value well below the maximum is demonstrated in the following.

Our results for the Kibble-Zurek scaling are based primarily on the excess energy. Three states emerge in the error analysis: (i) the ground state serving as the initial state to the quench; (ii) the ground state of the final parameters of the quench; and (iii) the final state of the quench. These three values are sufficient to track down the main source of error. Figure 11 shows the convergence of the energy measurements, which are the foundation of the excess energy. We varied the bond dimension from 25 to 1000. In addition, we show the difference from the simulation with the highest bond dimension. The convergence for the simulated bond dimension is straightforward. The remaining error of the order of 10^{-15} is an artifact of the machine precision in numerical simulations. This short error analysis justifies us in dismissing error bars from the numerical simulations in the fitting procedure for the Kibble-Zurek scaling.

V. CONCLUSION

We have examined the effects of linear quenches across quantum critical points in the BBM with a quadratic Zeeman field. Our primary focus has been to quench into the Haldane phase from phases which can be readily prepared in experiments, such as the Néel and large- D phases. We evaluated the validity of the Kibble-Zurek mechanism in each of these transitions by studying excess energy and different observables which are related to the correlation length as a function of quench time, such as the block entropy and the Schmidt gap. We base our results on numerical simulations with matrix product states methods in 1-dimensional finite-size systems.

For the Néel to Haldane phase transition, we found Kibble-Zurek-like power-law behavior in the excess energy. However, the behavior of the excess energy, along with the power-law exponent, depends on the quench protocol, i.e., whether we perform the quench along the external magnetic field, D , or interaction parameter, θ . The Schmidt gap and block entropy show signs of dynamical phase transitions through the appearance of cusps at specific quench times. The power-law exponent derived from the behavior of excess energy follows the Kibble-Zurek mechanism if the correct critical exponents are considered.

We find that the behavior of string order depends heavily on the quench protocol, with a marked difference in the two scenarios. Quenching across θ reveals a regime for quench times in which the final time-evolved string order is larger than the final ground state string order, suggesting the formation of defects due to the quench which not only preserves the string order, but also enhances it. Furthermore, the behavior of string order as a function of quench times shows almost no dependence on the system size. Quenching from the large- D to the Haldane phase shows yet again the dependence on the quench direction in the phase diagram. The string order shows a clear system-size dependence, with larger systems needing longer times for the final time-evolved string order to become approximately equal to the final ground state value. Our observations of the string order following a linear quench across the two quantum phase transitions will play an important role in experiments in search of the elusive Haldane phase.

We have seen that the investigation of the transitions to the Haldane phase yields intriguing physics. These results raise the question of which other phenomena the remaining phase transitions in the BBM may contain. These transitions are a fruitful subject for future studies. Second, it would be important to eventually model the system as an open system coupled to a reservoir, e.g., a with a Lindblad master equation in order to examine the question of decoherence in quantum simulators seeking to identify and explore the Haldane phase. Finally, a remaining open question is which cause for defects, i.e., the quench rate or the open system effects, is predominant for a given parametrization of the system.

ACKNOWLEDGMENTS

We thank J. R. Glick, L. Santos, G. Shchedrin, and M. L. Wall for useful discussions. This work was performed with partial support of the US National Science Foundation under Grants OAC-1740130, PHY-1806372, CCF-1839232, and DGE-2125899. We acknowledge support of the UK Engineering and Physical Sciences Research Council (EPSRC) through the Quantum Science with Ultracold Molecules Programme (Grant No. EP/P01058X/1). The authors acknowledge Colorado School of Mines supercomputing resources [69] made available for conducting the research reported in this paper.

-
- [1] E. Altman, K. R. Brown, G. Carleo, L. D. Carr, E. Demler, C. Chin, B. DeMarco, S. E. Economou, M. A. Eriksson, K.-M. C. Fu *et al.*, Quantum simulators: Architectures and opportunities, *PRX Quantum* **2**, 017003 (2021).
 - [2] R. P. Feynman, Simulating physics with computers, *Int. J. Theor. Phys.* **21**, 467 (1982).
 - [3] T. Albash and D. A. Lidar, Adiabatic quantum computation, *Rev. Mod. Phys.* **90**, 015002 (2018).
 - [4] Z.-C. Gu and X.-G. Wen, Tensor-entanglement-filtering renormalization approach and symmetry-protected topological order, *Phys. Rev. B* **80**, 155131 (2009).
 - [5] T. Senthil, Symmetry-protected topological phases of quantum matter, *Annu. Rev. Condens. Matter Phys.* **6**, 299 (2015).
 - [6] F. D. M. Haldane, Continuum dynamics of the 1-D Heisenberg antiferromagnet: Identification with the O(3) nonlinear sigma model, *Phys. Lett. A* **93**, 464 (1983).
 - [7] D. V. Else, I. Schwarz, S. D. Bartlett, and A. C. Doherty, Symmetry-Protected Phases for Measurement-Based Quantum Computation, *Phys. Rev. Lett.* **108**, 240505 (2012).
 - [8] D. T. Stephen, D.-S. Wang, A. Prakash, T.-C. Wei, and R. Raussendorf, Computational Power of Symmetry-Protected Topological Phases, *Phys. Rev. Lett.* **119**, 010504 (2017).
 - [9] D. Bacon, S. T. Flammia, and G. M. Crosswhite, Adiabatic Quantum Transistors, *Phys. Rev. X* **3**, 021015 (2013).
 - [10] D. J. Williamson and S. D. Bartlett, Symmetry-protected adiabatic quantum transistors, *New J. Phys.* **17**, 053019 (2015).
 - [11] S. D. Bartlett, G. K. Brennen, and A. Miyake, Robust symmetry-protected metrology with the haldane phase, *Quantum Sci. Technol.* **3**, 014010 (2018).
 - [12] J. P. Ronzheimer, M. Schreiber, S. Braun, S. S. Hodgman, S. Langer, I. P. McCulloch, F. Heidrich-Meisner, I. Bloch, and U. Schneider, Expansion Dynamics of Interacting Bosons in Homogeneous Lattices in One and Two Dimensions, *Phys. Rev. Lett.* **110**, 205301 (2013).
 - [13] S. Scherg, T. Kohlert, J. Herbrych, J. Stolpp, P. Bordia, U. Schneider, F. Heidrich-Meisner, I. Bloch, and M. Aidelsburger, Nonequilibrium Mass Transport in the 1D Fermi-Hubbard Model, *Phys. Rev. Lett.* **121**, 130402 (2018).
 - [14] T. Kinoshita, T. Wenger, and D. S. Weiss, A quantum Newton's cradle, *Nature (London)* **440**, 900 (2006).
 - [15] M. Schreiber, S. S. Hodgman, P. Bordia, H. P. Lüschen, M. H. Fischer, R. Vosk, E. Altman, U. Schneider, and I. Bloch, Observation of many-body localization of interacting fermions in a quasirandom optical lattice, *Science* **349**, 842 (2015).
 - [16] H. P. Lüschen, P. Bordia, S. S. Hodgman, M. Schreiber, S. Sarkar, A. J. Daley, M. H. Fischer, E. Altman, I. Bloch, and U. Schneider, Signatures of Many-Body Localization in a Controlled Open Quantum System, *Phys. Rev. X* **7**, 011034 (2017).
 - [17] M. Aidelsburger, J. L. Ville, R. Saint-Jalm, S. Nascimbène, J. Dalibard, and J. Beugnon, Relaxation Dynamics in the Merging of N Independent Condensates, *Phys. Rev. Lett.* **119**, 190403 (2017).
 - [18] G. Lamporesi, S. Donadello, S. Serafini, F. Dalfovo, and G. Ferrari, Spontaneous creation of Kibble-Zurek solitons in a Bose-Einstein condensate, *Nat. Phys.* **9**, 656 (2013).
 - [19] C. Meldgin, U. Ray, P. Russ, D. Chen, D. M. Ceperley, and B. DeMarco, Probing the Bose glass-superfluid transition using quantum quenches of disorder, *Nat. Phys.* **12**, 646 (2016).

- [20] C. Senko, P. Richerme, J. Smith, A. Lee, I. Cohen, A. Retzker, and C. Monroe, Realization of a Quantum Integer-Spin Chain with Controllable Interactions, *Phys. Rev. X* **5**, 021026 (2015).
- [21] L. D. Carr, D. DeMille, R. V. Krems, and J. Ye, Cold and ultracold molecules: Science, technology and applications, *New J. Phys.* **11**, 055049 (2009).
- [22] J. P. Covey, S. A. Moses, J. Ye, and D. S. Jin, Controlling a quantum gas of polar molecules in an optical lattice, in *Cold Chemistry: Molecular Scattering and Reactivity near Absolute Zero* (The Royal Society of Chemistry, London, 2017), Chap. 11, pp. 537–578.
- [23] W. S. Bakr, J. I. Gillen, A. Peng, S. Fölling, and M. Greiner, A quantum gas microscope for detecting single atoms in a Hubbard-regime optical lattice, *Nature (London)* **462**, 74 (2009).
- [24] J. F. Sherson, C. Weitenberg, M. Endres, M. Cheneau, I. Bloch, and S. Kuhr, Single-atom-resolved fluorescence imaging of an atomic Mott insulator, *Nature (London)* **467**, 68 (2010).
- [25] M. Endres, M. Cheneau, T. Fukuhara, C. Weitenberg, P. Schauß, C. Gross, L. Mazza, M. C. Bañuls, L. Pollet, I. Bloch, and S. Kuhr, Observation of correlated particle-hole pairs and string order in low-dimensional Mott insulators, *Science* **334**, 200 (2011).
- [26] A. Imambekov, M. Lukin, and E. Demler, Spin-exchange interactions of spin-one bosons in optical lattices: Singlet, nematic, and dimerized phases, *Phys. Rev. A* **68**, 063602 (2003).
- [27] T. Murashima and K. Nomura, Incommensurability and edge states in the one-dimensional $s = 1$ bilinear-biquadratic model, *Phys. Rev. B* **73**, 214431 (2006).
- [28] A. Läuchli, G. Schmid, and S. Trebst, Spin nematics correlations in bilinear-biquadratic $s = 1$ spin chains, *Phys. Rev. B* **74**, 144426 (2006).
- [29] K. Rodríguez, A. Argüelles, A. K. Kolezhuk, L. Santos, and T. Vekua, Field-Induced Phase Transitions of Repulsive Spin-1 Bosons in Optical Lattices, *Phys. Rev. Lett.* **106**, 105302 (2011).
- [30] G. De Chiara, M. Lewenstein, and A. Sanpera, Bilinear-biquadratic spin-1 chain undergoing quadratic Zeeman effect, *Phys. Rev. B* **84**, 054451 (2011).
- [31] P. J. Low, B. M. White, A. A. Cox, M. L. Day, and C. Senko, Practical trapped-ion protocols for universal qudit-based quantum computing, *Phys. Rev. Res.* **2**, 033128 (2020).
- [32] U. Schollwöck, The density-matrix renormalization group in the age of matrix product states, *Ann. Phys.* **326**, 96 (2011).
- [33] T. A. Hilker, G. Salomon, F. Grusdt, A. Omran, M. Boll, E. Demler, I. Bloch, and C. Gross, Revealing hidden antiferromagnetic correlations in doped Hubbard chains via string correlators, *Science* **357**, 484 (2017).
- [34] G. Vidal, J. I. Latorre, E. Rico, and A. Kitaev, Entanglement in Quantum Critical Phenomena, *Phys. Rev. Lett.* **90**, 227902 (2003).
- [35] J. Eisert, M. Cramer, and M. B. Plenio, Colloquium: Area laws for the entanglement entropy, *Rev. Mod. Phys.* **82**, 277 (2010).
- [36] C. Holzhey, F. Larsen, and F. Wilczek, Geometric and renormalized entropy in conformal field theory, *Nucl. Phys. B* **424**, 443 (1994).
- [37] V. E. Korepin, Universality of Entropy Scaling in One Dimensional Gapless Models, *Phys. Rev. Lett.* **92**, 096402 (2004).
- [38] P. Calabrese and J. Cardy, Entanglement entropy and quantum field theory, *J. Stat. Mech.: Theory Exp.* (2004) P06002.
- [39] P. Calabrese and J. Cardy, Entanglement entropy and conformal field theory, *J. Phys. A: Math. Theor.* **42**, 504005 (2009).
- [40] L. Lepori, G. De Chiara, and A. Sanpera, Scaling of the entanglement spectrum near quantum phase transitions, *Phys. Rev. B* **87**, 235107 (2013).
- [41] G. De Chiara, L. Lepori, M. Lewenstein, and A. Sanpera, Entanglement Spectrum, Critical Exponents, and Order Parameters in Quantum Spin Chains, *Phys. Rev. Lett.* **109**, 237208 (2012).
- [42] F. D. M. Haldane, Nonlinear Field Theory of Large-Spin Heisenberg Antiferromagnets: Semiclassically Quantized Solitons of the One-Dimensional Easy-Axis Néel State, *Phys. Rev. Lett.* **50**, 1153 (1983).
- [43] E. G. Dalla Torre, E. Berg, and E. Altman, Hidden Order in 1D Bose Insulators, *Phys. Rev. Lett.* **97**, 260401 (2006).
- [44] E. Berg, E. G. Dalla Torre, T. Giamarchi, and E. Altman, Rise and fall of hidden string order of lattice bosons, *Phys. Rev. B* **77**, 245119 (2008).
- [45] L. Mazza, D. Rossini, M. Endres, and R. Fazio, Out-of-equilibrium dynamics and thermalization of string order, *Phys. Rev. B* **90**, 020301 (2014).
- [46] M. Calvanese Strinati, L. Mazza, M. Endres, D. Rossini, and R. Fazio, Destruction of string order after a quantum quench, *Phys. Rev. B* **94**, 024302 (2016).
- [47] T. Caneva, R. Fazio, and G. E. Santoro, Adiabatic quantum dynamics of a random Ising chain across its quantum critical point, *Phys. Rev. B* **76**, 144427 (2007).
- [48] T. Caneva, R. Fazio, and G. E. Santoro, Adiabatic quantum dynamics of the Lipkin-Meshkov-Glick model, *Phys. Rev. B* **78**, 104426 (2008).
- [49] F. Pellegrini, S. Montangero, G. E. Santoro, and R. Fazio, Adiabatic quenches through an extended quantum critical region, *Phys. Rev. B* **77**, 140404(R) (2008).
- [50] A. Dhar, D. Rossini, and B. P. Das, Quasiadiabatic dynamics of ultracold bosonic atoms in a one-dimensional optical superlattice, *Phys. Rev. A* **92**, 033610 (2015).
- [51] T. W. B. Kibble, Topology of cosmic domains and strings, *J. Phys. A: Math. Gen.* **9**, 1387 (1976).
- [52] W. H. Zurek, Cosmological experiments in superfluid helium? *Nature (London)* **317**, 505 (1985).
- [53] W. H. Zurek, U. Dorner, and P. Zoller, Dynamics of a Quantum Phase Transition, *Phys. Rev. Lett.* **95**, 105701 (2005).
- [54] J. Dziarmaga, Dynamics of a quantum phase transition and relaxation to a steady state, *Adv. Phys.* **59**, 1063 (2010).
- [55] A. Polkovnikov, K. Sengupta, A. Silva, and M. Vengalattore, Colloquium: Nonequilibrium dynamics of closed interacting quantum systems, *Rev. Mod. Phys.* **83**, 863 (2011).
- [56] L. Cincio, J. Dziarmaga, M. M. Rams, and W. H. Zurek, Entropy of entanglement and correlations induced by a quench: Dynamics of a quantum phase transition in the quantum Ising model, *Phys. Rev. A* **75**, 052321 (2007).
- [57] E. Canovi, E. Ercolessi, P. Naldesi, L. Taddia, and D. Vodola, Dynamics of entanglement entropy and entanglement spectrum crossing a quantum phase transition, *Phys. Rev. B* **89**, 104303 (2014).

- [58] S. Sachdev, *Quantum Phase Transitions*, 2nd ed. (Cambridge University Press, Cambridge, 2011).
- [59] L. D. Carr, *Understanding Quantum Phase Transitions*, Condensed Matter Physics (CRC Press, Boca Raton, FL, 2010).
- [60] E. Canovi, D. Rossini, R. Fazio, and G. E. Santoro, Adiabatic dynamics in a spin-1 chain with uniaxial single-spin anisotropy, *J. Stat. Mech.: Theory Exp.* (2009) P03038.
- [61] N. V. Vitanov and B. M. Garraway, Landau-Zener model: Effects of finite coupling duration, *Phys. Rev. A* **53**, 4288 (1996).
- [62] N. V. Vitanov, Transition times in the Landau-Zener model, *Phys. Rev. A* **59**, 988 (1999).
- [63] A. Bermudez, D. Patanè, L. Amico, and M. A. Martin-Delgado, Topology-Induced Anomalous Defect Production by Crossing a Quantum Critical Point, *Phys. Rev. Lett.* **102**, 135702 (2009).
- [64] M. Heyl, A. Polkovnikov, and S. Kehrein, Dynamical Quantum Phase Transitions in the Transverse-Field Ising Model, *Phys. Rev. Lett.* **110**, 135704 (2013).
- [65] A. Mazurenko, C. S. Chiu, G. Ji, M. F. Parsons, M. Kanász-Nagy, R. Schmidt, F. Grusdt, E. Demler, D. Greif, and M. Greiner, A cold-atom Fermi-Hubbard antiferromagnet, *Nature (London)* **545**, 462 (2017).
- [66] OpenTEBD: Open Source Time-Evolving Block Decimation, <http://sourceforge.net/projects/opentebd>.
- [67] D. Jaschke, M. L. Wall, and L. D. Carr, Open source matrix product states: Opening ways to simulate entangled many-body quantum systems in one dimension, *Comput. Phys. Commun.* **225**, 59 (2018).
- [68] Open Source Matrix Product States (OpenMPS), <http://sourceforge.net/projects/openmps>.
- [69] See <https://ciarc.mines.edu/hpc>.